Cyclopentadienone-NHC iron(0) complexes as low valent electrocatalysts for water oxidation

Cyclopentadienone-NHC Iron(0) Complexes as Low Valent Electrocatalysts for Water Oxidation

Andrea Cingolani,[a] Isacco Gualandi,[a,b]* Erika Scavetta,[a,b] Cristiana Cesari,[a] Stefano Zacchini,[a] Domenica Tonelli,[a,b] Valerio Zanotti,[a,b] Paola Franchi,[c] Marco Lucarini,[c] Emilia Sicilia,[d] Gloria Mazzone,[d] Daniele Nanni,[a] and Rita Mazzoni[a,b]*

The design and development of stable molecular iron electrocatalysts able to work with low overpotential in the oxidation of water to molecular oxygen is an essential challenge for sustainable energy applications. Our group has recently developed stable iron(0) *N*-heterocyclic carbene (NHC) complexes bearing a non-innocent cyclopentadienone (Cp=O) ligand. This peculiar ligands combination is herein exploited to tune the electrochemistry of the corresponding complexes: NHCs regulate the anodic process in a suitable potential region for oxidation of water to O_2 and cyclopentadienone promotes a mono-electronic redox process through the formation of a radical complex (**1•**). The synergic effect of these ligands on iron complexes makes them suitable, for the first time, as low valent electrocatalysts for water oxidation. The electrocatalytic activity was determined in water/THF with added KOH. Complex **1** shows the best catalytic activity and competitive efficiency in terms of both TOF (up to 52 s^{-1}) and overpotential (320 mV).

Introduction

Artificial photosynthesis, the sunlight-driven splitting of water in molecular hydrogen and oxygen, shows its bottleneck in water oxidation to O_2:[1-4] hence the challenge of finding highly efficient, selective, stable water oxidation catalysts (WOCs). In the last decade a considerable effort has been devoted to homogeneous molecular water oxidation catalysts (MWOCs),[5,6] mainly based on Ru,[7-11] Ir,[12-15] Co,[16-19] Cu,[20-25] and Mn[26-30] mono- or multinuclear complexes. Despite the long-standing comparison with heterogeneous catalysis, advances in the field were boosted due to their flexibility in tuning and optimizing reactivity and redox properties by ligand rational design, with the principal aim to obtain catalysts with good activity and, above all, low overpotential, that is the essential parameter for industrial applications.

In the search for efficient and robust catalysts based on abundant, affordable first-row transition metals, iron based MWOC catalysts are crucially important[31,32] since they can pave the way for the realization of economically viable water splitting processes as competitive green alternative for energetic applications.[33-35] The history of iron-based MWOCs, assisted by sacrificial oxidants such as cerium ammonium nitrate (CAN) or $NaIO_4$,[36] began in 2010 with the pioneering work of Bernhard et al.[37] dealing on iron-based MWOCs bearing tetra-amide macrocyclic ligands (TAMLs) able to hold high-valent metal ions. TAMLs were subsequently modified by Dahr et al. with the biuret–amide group.[38,39] On the other hand, families of non-heme multidentate coordination complexes[40] soon displayed far better catalytic performances in water oxidation, with a turnover number (TON) of 1000[41] and a turnover frequency (TOF) of 2.2 s^{-1}.[42] The main series of iron based MWOCs are typical non-heme iron complexes able to generate and stabilize high-valent iron oxo species. It is also relevant the use of a di- or multi-nuclear complex to facilitate O-O bond formation through bridging oxygen. On the other hand, O-O bond formation can also involve a radical coupling mechanism.[43-48]

Sacrificial oxidants have been recently demonstrated to be not only simply innocent one-electron acceptors, but they can also intervene in some way in the reaction mechanism.[36] Hence, an increased interest is nowadays oriented on a cleaner way to transfer electrons, i.e. electrocatalysis, which avoids the harsh oxidative conditions, reducing catalyst deactivation and improving, in principle, manageability and tunability of the reaction. Furthermore, although limited in number, iron based WOCs molecular electrocatalysts are closer to the aim of using MWOCs in artificial photosynthesis.[49]

The first well-defined electrocatalytic iron based MWOC has been reported by Meyer et al.: it involved the generation, in propylene carbonate, of the Fe(V)=O species, which was subsequently attacked by H_2O as the limiting reagent.[50] The best single-site electrocatalyst appeared to be the pentanuclear iron complex reported by Masaoka and co-workers, which performs water oxidation with the highest TON and TOF of 10^7 and 1400 s^{-1}, respectively.[51] Each Fe(II)/Fe(III) couple undergoes five reversible waves representing the five sequentially occurring one-electron redox reactions. The same authors also reported on the tunability of overpotential and TOF by ligand design.[36] Nevertheless, in 2020, Llobet and co-workers demonstrated iron oxide particles, formed due to complex decomposition, as the actual catalyst in the latter case.[52] Hetterscheid et al.[53] have instead reported on the influence of the electrode material (e.g., graphitic vs. gold working) on the catalytic performances of electrochemical water oxidation

driven by a binuclear homogeneous catalyst. These results were further implemented in 2020 by a ligand design that improved the whole efficiency of dinuclear oxo-bridged iron MWOCs in organic solvents with NaOH as the source of oxygen.[54] As far as water soluble MWOCs are concerned, Zhan et al. have reported sustainable water oxidation catalysis at an indium tin oxide (ITO),[55] although Najafpour et al. lately suggested that even in this case, water oxidation should be ascribed to the formation of heterogeneous iron oxide.[56]

Our group has recently developed an easy synthetic pathway for the synthesis of a family of iron(0) cyclopentadienone (Cp=O) and *N*-heterocyclic carbene (NHC) complexes.[57] This ligands combination is here exploited for the preparation of a series of complexes employed for the first time as suitable MWOC catalysts that, under basic conditions, show competitive efficiency in terms of both TOF and overpotential. Indeed, neither NHC iron complexes,[58] nor cyclopentadienone[59,60] ones have been previously reported as active MWOC catalysts. It is worth pointing out that both ligands play a key role in the electrochemistry of the whole system: the former shifts the anodic process in a potential region suitable for oxidation of water to O_2, the latter favours a mono-electronic redox route, as demonstrated by isolation of a radical complex from an exhaustive mono-electronic oxidation (**1•**). Electrochemistry and catalytic activity are also influenced by substituents in both cyclopentadienone and NHC ligands.

Experimental

Materials and methods

All reactions were routinely carried out under a nitrogen atmosphere, using standard Schlenk techniques. Glassware was oven dried before use. Solvents: dichloromethane (CH_2Cl_2), tetrahydrofuran (THF), diethyl ether (Et_2O), petroleum ether (referring to a fraction of bp 60-80 °C), and acetonitrile (CH_3CN) were dried and distilled prior to use. Other solvents such as ethyl acetate (EtOAc), methanol (MeOH), toluene, and $CDCl_3$ (Sigma Aldrich) were employed without further purification. Reagents: $Fe_2(CO)_9$ (Strem), methyl iodide, silver oxide, 1-methylimidazole, trifluoroboric acid, octa-1,7-dyine, dipropargyl ether, (Alpha Aesar) were used as purchased. 1,3-Dimethylimidazolium iodide,[61] 1-methyl-3-(2-hydroxypropyl)imidazolium bromide, 1,8-bis(trimethylsilyl)octa-1,7-diyne, (oxybis(prop-1-yne-3,1-diyl))bis(trimethylsilane),[62] triscarbonyl-(2,4-bis(trimethylsilyl)bicyclo[3.3.0]nona-1,4-dien-3-one)iron (**6**), dicarbonyl-(2,4-bis(trimethylsilyl)bicyclo[3.3.0]nona-1,4-dien-3-one)[1,3-dimethyl-ilidene]iron(**1**), dicarbonyl-(2,4-bis(trimethylsilyl)bicyclo[3.3.0]nona-1,4-dien-3-one)[1-(2-BocNH-ethyl)-3-methylilidene]iron (**2-BoC**),[63] dicarbonyl-(2,4-bis(trimethylsilyl)bicyclo[3.3.0]nona-1,4-dien-3-one)[1-(2-aminoethyl)-3-methylilidene]iron (**2**),[63] and triscarbonyl-(4,6-bis(trimethylsilyl)-*1H*-cyclopenta[c]furan-5(*3H*)-one)iron,[64] were prepared following procedures reported in the literature. NMR spectra were recorded using Varian Inova 300 (^{1}H, 300.1; ^{13}C, 75.5 MHz), Varian Mercury Plus VX 400 (^{1}H, 400; ^{13}C, 100.6 MHz), and Varian Inova 600 (^{1}H, 599.7; ^{13}C, 151 MHz) spectrometers at 298 K; chemical shifts were referenced internally to residual solvent peaks. Infrared spectra were recorded at 298 K on a Perkin-Elmer Spectrum Two spectrophotometer. ESI-MS spectra were recorded on a Waters Micromass ZQ 4000 instrument with samples dissolved in MeOH or CH_3CN. Elemental analyses were performed with a Thermo Scientific Flash 2000 instrument equipped with a CHNS analyser.

Dicarbonyl-(2,4-bis(trimethylsilyl)bicyclo[3.3.0]nona-1,4-dien-3-one)[1-(3-hydroxypropyl)-3-methylilidene]iron (3). In a dried 100 mL Schlenk flask, triscarbonyl-(2,4-bis(trimethylsilyl)bicyclo[3.3.0]nona-1,4-dien-3-one)iron (**6**) (0.048 g, 0.103 mmol), trimethylammine-*N*-oxide (0.012 g, 0.155 mmol), 3-(2-hydroxypropyl)-1-methylimidazole bromide (0.022 g, 0.103 mmol), and silver oxide (0.037 g, 0.160 mmol) were added to the reaction vessel and dissolved in acetonitrile (8 mL). The reaction mixture was stirred at room temperature and protected from light for 3 hours. Solvent was removed in vacuo. The solid was re-dissolved in toluene (20 mL) and stirred under reflux for 1 hour. At the end the solvent was removed under vacuum and the crude was purified to afford the yellow iron complex **3** by column chromatography on neutral alumina using dichloromethane/ethyl acetate/MeOH (100/0/0 to 0/0/100). Yield = 45 mol%. **3** was analyzed by IR, ^{1}H-NMR, ^{13}C-NMR, and ESI-MS. ^{1}H-NMR (400 MHz, 298 K, $CDCl_3$) δ (ppm): 7.10 (s, 1H, -CH_{NHC}), 7.02 (s, 1H, -CH_{NHC}), 4.36 (t, $J_{H,H}$ = 4.0 Hz, CH_2, NHC), 3.89 (s, 6H, -NCH_3), 3.71 (t, $J_{H,H}$ = 4.0 Hz, 2H, -CH_2, NHC), 2.44 (t, $J_{H,H}$ = 4.0 Hz, 4H, CH_2), 2.12-2.09 (m, 2H, CH_2), 1.88-1.84 (m, 2H, CH_2), 1.84-1.51 (m, 2H, CH_2), 0.16 (s, 18H, CH_3, TMS). ^{13}C-NMR (151 MHz, 298 K, $CDCl_3$, g-HSQC, g-HMBC) δ (ppm): 218.0 (CO), 183.2 ($C_{carbene}$), 175.0 (C=O, Cp), 123.9 (CH_{NHC}), 122.3 (CH_{NHC}), 103.6 ($C_{3,4}$, Cp), 72.1 ($C_{2,5}$, Cp), 58.7 (-CH_2O-), 48.4 (-NCH_2), 48.4 (-NCH_3), 32.9 (-CH_2-), 24.8 (-CH_2), 22.5 (-CH_2), 0.1 (CH_3, TMS). IR (CH_2Cl_2, cm^{-1}): (ν_{CO}) 1984, 1924. ESI-MS (m/z): 531 $[M+H]^+$, 553 $[M+Na]^+$. Anal. Calcd (%) for $C_{24}H_{38}N_2O_4Si_2Fe$: C, 54.33; H, 7.22; N, 5.28. Found: C, 54.34; H, 7.22; N, 5.26.

Dicarbonyl-(4,6-bis(trimethylsilyl)-*1H*-cyclopenta[c]furan-5(*3H*)-one)[1,3-dimethylilidene] iron (4). In a dried 100 mL Schlenk flask, 1,3-dimethylimidazolium iodide (0.116 g, 0.52 mmol), silver oxide (0.132 g, 0.57 mmol), triscarbonyl-(4,6-bis(trimethylsilyl)-*1H*-cyclopenta[c]furan-5(*3H*)-one)iron (0.200 g, 0.48 mmol) and trimethylammine-*N*-oxide (0.054 g, 0.72 mmol) were added to the reaction vessel and dissolved in acetonitrile (8 mL). The reaction mixture was stirred at room temperature and protected from light for 1 hour. Solvent was removed in vacuum. The solid was re-dissolved in toluene (20 mL) and stirred under reflux for 1 hour. At the end the solvent was removed under vacuum and the crude was purified to afford the yellow iron complex **4** by column chromatography on neutral alumina using dichloromethane/ethyl acetate (100 to 100). Yield = 54 mol%. **4** was analyzed by IR, ^{1}H-NMR, ^{13}C-NMR, and ESI-MS. ^{1}H-NMR (400 MHz, 298 K, $CDCl_3$) δ (ppm): 6.97 (s, 2H, CH_{im}), 4.59 (dd, $J_{1H,H}$ = 56 Hz, $J_{2H,H}$ = 12 Hz, 4H, CH_2), 3.86 (s, 3H, NCH_3), 0.12 (s. 18H, -CH_{3TMS}). ^{13}C-NMR (151 MHz, 298 K, $CDCl_3$)

δ (ppm): 216.1 (CO), 182.5 (C_{carb}), 181.1 (C=O, Cp), 124.1 (CH_{im}), 108.8 ($C_{2,5}$, Cp), 68.1 (CH_2) 63.4 ($C_{3,4}$, Cp), 39.2 (NCH_3), -0.7 (CH_{3TMS}). IR (CH_2Cl_2, cm^{-1}): (ν_{CO}) 1991, 1931. ESI-MS (m/z): 419 $[M-2CO+H]^+$, 447 $[M-CO+H]^+$, 475 $[M+H]^+$, 497 $[M+Na]^+$, 513 $[M+K]^+$. Anal. Calcd (%) for $C_{20}H_{30}N_2O_4Si_2Fe$: C, 50.63; H, 6.37; N, 5.90. Found: C, 50.50; H, 6.22; N, 5.76.

Dicarbonyl-(4,6-bis(trimethylsilyl)-*1H*-cyclopenta[c]furan-5(*3H*)-one)[1-(2-BocNH-ethyl)-3-methylilidene] iron (5-Boc). In a dried 100 mL Schlenk flask, 1-(2-BocNH-ethyl-)-3-methylimidazolium iodide (0.200 g, 0.57 mmol), silver oxide (0.153 g, 0.66 mmol), triscarbonyl-(4,6-bis(trimethylsilyl)-*1H*-cyclopenta[c]furan-5(*3H*)-one)iron (0.220 g, 0.55 mmol), and trimethylammine-*N*-oxide (0.062 g, 0.83 mmol) were added to the reaction vessel and dissolved in acetonitrile (10 mL). The reaction mixture was stirred at room temperature and protected from light for 1 hour. Solvent was removed in vacuo. The solid was re-dissolved in toluene (20 mL) and stirred under reflux for 1 hour. At the end the solvent was removed under vacuum and the crude was purified to afford the yellow iron complex **5-Boc** by column chromatography on neutral alumina using dichloromethane/ethyl acetate (100 to 100). Yield = 51 mol% **5-Boc** was analyzed by IR, ^{1}H-NMR, ^{13}C-NMR, and ESI-MS. ^{1}H-NMR (400 MHz, 298 K, $CDCl_3$) δ (ppm): 7.13 (s, 1H, CH_{im}), 7.10 (s, 1H, CH_{im}), 4.59 (dd, $J_{1H,H}$ = 56 Hz, $J_{2H,H}$ = 12 Hz, 4H, CH_2), 4.38-4.32 (m, 2H, CH_2) 3.84 (s, 3H, NCH_3), 3.53-3.48 (m, 2H, CH_2), 1.43 (s, 9H, BOC), 0.13 (s, 18H, CH_{3TMS}). ^{13}C-NMR (151 MHz, 298 K, $CDCl_3$) δ (ppm): 216.6 (CO), 182.6 (C_{carb}), 180.7 (C=O, Cp), 156.1 (C=O, BOC), 124.6 (CH_{im}), 122.5 (CH_{im}), 108.8 ($C_{2,5}$, Cp), 79.8 (C_{BOC}), 68.1 (CH_2), 64.5 ($C_{3,4}$, Cp), 50.6 (CH_2), 40.8 (CH_2), 39.1 (NCH_3), 28.3 ($CH_{3,BOC}$), -0.7 (CH_{3TMS}). IR (CH_2Cl_2, cm^{-1}): (ν_{CO}) 1990, 1932; ($\nu_{C=O,BOC}$) 1712; ($\nu_{C=O}$) 1578. ESI-MS (m/z): 604 $[M+H]^+$, 626 $[M+Na]^+$, 642 $[M+K]^+$. Anal. Calcd (%) for $C_{26}H_{41}N_3O_6Si_2Fe$: C, 51.73; H, 6.85; N, 6.96. Found: C, 51.86; H, 6.92; N, 7.07.

Dicarbonyl-(4,6-bis(trimethylsilyl)-*1H*-cyclopenta[c]furan-5(*3H*)-one)[1-(2-aminoethyl)-3-methylilidene] iron (5). In a dried 25 mL Schlenk flask, **5-Boc** (0.146 g, 0.24 mmol) was dissolved in Et_2O (15 mL) and HBF_4 (0.16 mL, 1.2 mmol) was added dropwise. The reaction mixture was stirred at room temperature for 1 hour. The precipitate was filtrated and then dissolved in CH_2Cl_2, and the excess of HBF_4 neutralized with a saturated solution of sodium carbonate (pH ca. 8). The aqueous phase was extracted with CH_2Cl_2 and washed with potassium hydroxide solution (2M, 3x10 mL). The organic phase was dried with magnesium sulfate and filtrated. The solvent was removed to leave **5** as a yellow solid. Yield = 80 mol%. **5** was analyzed by IR, ^{1}H-NMR, ^{13}C-NMR, and ESI-MS. ^{1}H-NMR (400 MHz, 298 K, $CDCl_3$) δ (ppm): 7.18 (s, 1H, CH_{im}), 6.99 (s, 1H, CH_{im}), 4.59 (dd, $J_{1H,H}$ = 56 Hz, $J_{2H,H}$ = 12 Hz, 4H, CH_2), 4.27-4.23 (m, 2H, CH_2)., 3.85 (s, 3H, NCH_3), 3.11-3.07 (m, 2H, CH_2), 0.12 (s, 18H, CH_{3TMS}). ^{13}C-NMR (151 MHz, 298 K, $CDCl_3$) δ (ppm): 216.5 (CO), 182.4 (C_{carb}), 181.0 (C=O, Cp), 124.4 (CH_{im}), 122.7 (CH_{im}), 108.9 ($C_{2,5}$, Cp), 68.1 (CH_2), 63.7 ($C_{3,4}$, Cp), 53.8 (CH_2), 42.9 (CH_2), 39.0 (NCH_3), -0.7 (CH_{3TMS}). IR (CH_2Cl_2, cm^{-1}): (ν_{CO}) 1991, 1933; ($\nu_{C=O}$) 1605. ESI-MS (m/z): 504 $[M+H]^+$, 526 $[M+Na]^+$. Anal. Calcd (%) for $C_{21}H_{33}N_3O_4Si_2Fe$: C, 50.09; H, 6.61; N, 8.35. Found: C, 50.15; H, 6.54; N, 8.42.

Synthesis of 1•. To a solution of iron complex **1** (0.035 g, 0.07 mmol) in distilled THF (2 mL), contained in a dried 100 mL Schlenk flask, magic blue (0.060 g, 0.07 mmol) was slowly added. The reaction mixture was stirred at room temperature for 5 minutes. Hexane was added to the solution until a yellow solid precipitated. The supernatant was removed and the solid washed several times with hexane. Yield = 86 mol%. **1•** was analysed by IR, ^{1}H-NMR, ESI-MS, and EPR (*vide infra*). ^{1}H-NMR (400 MHz, THF-d_8) δ (ppm): 7.60 (br, CH_{im}), 4.03 (br, NCH_3), 2.50 (br, CH_2) 2.04 (br, CH_2) 0.11 (br, CH_{3TMS}). IR (THF, cm^{-1}): (ν_{CO}) 2023, 1974 cm^{-1}. ESI-MS (m/z): 335 $[SbCl_6]^-$, 486 $[M+H]^+$, 686 [M + PBN + Na]$^+$. Anal. Calcd (%) for $C_{22}H_{34}N_2O_3Si_2Fe$: C, 54.31; H, 7.04; N, 5.76. Found: C, 54.34; H, 7.12; N, 5.61.

1• reduction with sodium napthalenide. To a solution of iron complex **1•** (0.035 g, 0.07 mmol) in distilled THF (5 mL), contained in a dried 100 mL Schlenk flask, a solution of sodium napthalenide in THF (0.06M, 1 eq.) was added dropwise. The reaction mixture was stirred at room temperature until the deep green solution of sodium napthalenide disappeared. The solvent was removed under vacuum and the residue chromatographed over a pad of Alumina (EtOAc as eluent). Complex **1** was obtained as a yellow solid.

Electronic paramagnetic resonance (EPR) measurements.

Crystals or dissolved crystals in THF of samples were transferred in a sealed calibrated capillary glass tube, which was placed inside the thermostated (room temperature) cavity of a Bruker ELEXSYS E500 spectrometer equipped with a NMR gaussmeter to calibrate the magnetic field and a frequency counter to determine the *g*-factors, which were corrected against the perylene radical cation in concentrated sulfuric acid (*g* = 2.002583). The following EPR instrument settings were used: modulation amplitude = 10.0 G; conversion time = 163.84 ms; time constant = 163.84 ms; modulation frequency 100 kHz; microwave power = 6.4 mW. The EPR spectrum of the solid samples shows a paramagnetic resonance peak with a Landé factor *g* = 2.01889 and a line width of 197.20 Gs. The EPR spectrum of the dissolved samples shows a paramagnetic resonance peak with a Landé factor *g* = 2.01247 and a line width of 44.66 Gs.

Electrochemical Characterisation.

Cyclic voltammograms were recorded at a scan rate of 0.05 V s^{-1} on a BAS-100A electrochemical analyser using a three-electrode cell with a glassy-carbon disk (0.071 cm^2) as the working electrode, a $Ag/AgNO_3$ (0.1 M) as the reference electrode, and a platinum-wire as the counter electrode. All experiments were performed under nitrogen atmosphere in CH_3CN containing 0.1 M $^nBu_4NPF_6$ at room temperature. Ferrocene (Fc) was the internal reference, and all potentials have been quoted relative to the Fc/Fc^+ couple set at 0.00 V.

Electrocatalytic Experiments. Cyclic voltammograms were recorded with the same setup of characterisation, but in THF/H_2O (4:1) mixture. Potassium hydroxide was added in molar equivalent increments via a micropipette. All CVs have

been recorded starting from the open circuit potential. Plot of i_{cat}/i_b vs KOH concentration showed an almost linear increment of current following base addition.

X-Ray diffraction studies

Crystal data and collection details for **4** are reported in Table S1. The diffraction experiments were carried out on a Bruker APEX II diffractometer equipped with a PHOTON100 detector using Mo–Kα radiation. Data were corrected for Lorentz polarization and absorption effects (empirical absorption correction SADABS).[65] Structures were solved by direct methods and refined by full-matrix least-squares based on all data using F^2.[66] All hydrogen atoms were fixed at calculated positions and refined by a riding model. All non-hydrogen atoms were refined with anisotropic displacement parameters.

Computational Details

All the structures were optimized at the Density Functional Theory level employing the B3LYP exchange–correlation functional by using the Gaussian09 package.[67] The 6-31++G** basis set was used for all the atoms except iron, for which the relativistic compact Stuttgart/Dresden effective core potential was used in conjunction with its split valence basis set.[68] Harmonic vibrational frequency calculations have been performed to confirm all the optimized structures as actual minima. Unrestricted approach was used for the accurate calculation of the open-shell system, **1•**, and no spin contamination was found ($\langle S^2 \rangle = 0.75$).

NBO charge analysis was carried out on the optimized structures of the investigated iron complexes.[69]

Results and discussion

Iron complexes employed in this work as electrocatalysts for water oxidation are summarized in Chart 1. Complexes **1**,[57] **2**,[63] **3**, **4**, and **5** were prepared following a synthetic strategy of our group.[57,70] A complete description of the synthesis and characterization of novel complexes **3**, **4**, and **5** is available in the experimental and SI (Figure S10-S21).

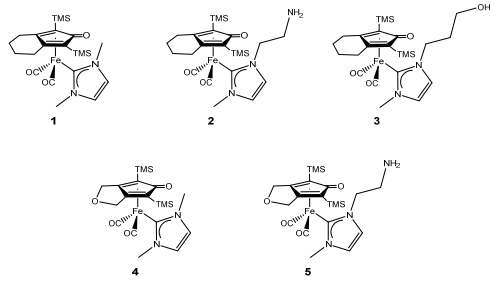

Chart 1. Cyclopentadienone-NHC iron(0) complexes investigated as electrocatalysts for water oxidation.

NMR spectra of **3**, **4**, and **5** were consistent with those of the previously reported **1** and **2**: in particular, ^{13}C-NMRs show the diagnostic signal of the Fe-$C_{carbene}$ moiety in the typical 182-183 ppm region. Spectral data comparison between complexes **1** and **4,** containing the same NHC ligand but different cyclopentadienones, indicates an increasing electron-withdrawing character of the furan ring of **4**: this is suggested by the lower back-bonding of carbonyl ligands showed by IR spectra (**1** ν(CO) = 1983, 1922 cm^{-1}; **4** ν(CO) = 1991, 1931 cm^{-1}) and, in the ^{13}C-NMR spectra, by the chemical shifts of the quaternary $C_{3,4}$, which result de-shielded passing from **1** (103.72 ppm) to **4** (108.80 ppm) due to removal of electron density.

The molecular structure of **4** was determined by X-ray crystallography (Figure 1). Suitable crystals were obtained by CH_2Cl_2/hexane double layer. The bonding parameters and overall structure of **4** is similar to those reported in the literature for related Fe and Ru complexes.[57, 63] In particular, the Fe(1)-C(3) distance [2.376(3) Å] is significantly longer than Fe(1)-C(4-7) [2.072(3)- 2.171(3) Å, average 2.118(6) Å] and C(3)-O(3) [1.241(4) Å] corresponds essentially to a double bond.[71] The Fe(1)-C(21) bond [1.978(3) Å] is in the typical range for the interaction between Fe(0) and a *N*-heterocyclic carbene.[72]

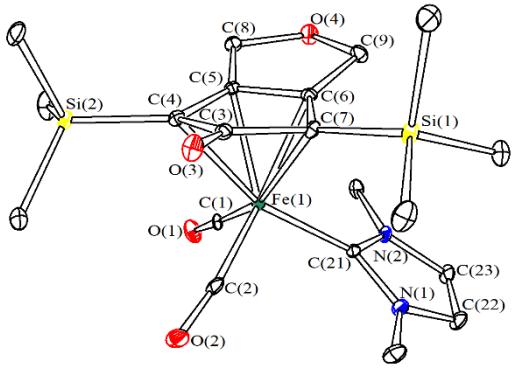

Figure 1. ORTEP drawing of **4**. Displacement ellipsoids are at the 30% probability level. H-atoms have been omitted for clarity. Selected bond lengths (Å): Fe(1)-C(1) 1.766(4), Fe(1)-C(2) 1.778(4), Fe(1)-C(3) 2.376(3), Fe(1)-C(4) 2.139(3), Fe(1)-C(5) 2.072(3), Fe(1)-C(6) 2.073(3), Fe(1)-C(7) 2.171(3), Fe(1)-C(21) 1.978(3), C(3)-O(3) 1.241(4), C(4)-Si(2) 1.866(4), C(7)-Si(1) 1.868(4), C(21)-N(1) 1.362(4), C(21)-N(2) 1.366(4), N(1)-C(22) 1.384(5), N(2)-C(23) 1.382(4), C(22)-C(23) 1.335(6).

Redox properties

In order to evaluate the influence of the cyclopentadienone, carbonyl, and NHC ligand combination, electrochemical properties of **1**-**5** were studied by cyclic voltammetry in deaerated CH_3CN containing Bu_4NPF_6 (0.1 M) (Figure 2). The nature of the ligands was found to affect both the potentials and the reversibility of the redox processes. All compounds display at least one oxidation wave. The formal half-wave potentials of the reversible processes and the peak potentials of the irreversible ones are reported in Table 1.

The CV of complex **1** (black line in Figure 2) displays one reversible redox process in the anodic region with formal potential of +0.16 V versus ferrocenium/ferrocene (Fc^+/Fc). Furthermore, the reversible oxidation of **1**, surprisingly, revealed to be a one electron process, as suggested by the difference between the anodic and cathodic peak potentials, which is equal to 77 mV. Therefore, the iron centre is formally involved in the redox reaction as a Fe(0)/Fe(I) redox couple. This demonstrates that the NHC ligand, generally behaving as a good sigma donor,[73] provides intriguing redox properties to complex **1**: this is clearly further evidenced by comparison with the tris-carbonyl iron cyclopentadienone analogue **6**, for which one irreversible redox process at +1.15 V is registered under the same conditions (Figure S1).

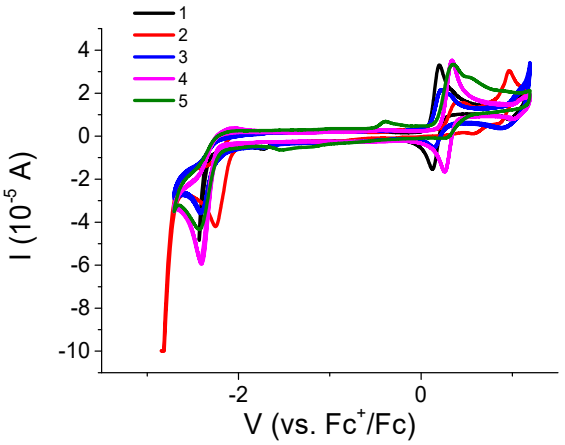

Figure 2. CVs recorded in a 2 mM CH_3CN solution of complexes **1-5**. Scan rate: 50 mVs^{-1}.

All the relevant redox processes of complexes **1-5** are reported in Table 1. Noteworthy, compounds **3** and **4** display the same behaviour as **1** in the anodic side with reversible systems, whose E_{ox}°' potentials are 0.19 and 0.31 V, respectively, in agreement with the higher electron withdrawing character of the furan substituted cyclopentadienone ligand (**4**). On the other hand, complexes **2** and **5**, bearing a NH_2 in the lateral chain of the NHC ligand, show two irreversible waves at +0.40 V and +0.97 V (Figure 2) and one at +0.35 V, respectively, in the anodic side. This different behaviour is related to the NH_2 group, whose presence causes the occurrence of a chemical reaction (EC mechanism). NH_2, as a reactive substituent, could be involved in basic or nucleophilic reactions, as well as in some interactions due to hydrogen bonds. Furthermore, CO release, favoured by the coordinating amino group, was already observed.[63] In order to shed some light on the peculiar behaviour of complexes **2** and **5**, CV of **2** was also recorded in phosphate buffer aqueous solution at pH 2 (Figure 3). Under these conditions **2** is soluble in water and the amino group is totally protonated, hence being unsusceptible to be involved in any side reactions. Indeed, CV showed only one reversible redox process at +0.70 V, even at slow scan rates (5 mVs^{-1}), confirming the role of the NH_2 moiety in CH_3CN solution (Figure 3).

Table 1. Formal potentials of redox processes involving NHC-Cp=O iron complexes in acetonitrile.[a]

Complex	E_{red}°' (V vs. Fc^+/Fc)	E_{ox}°' (V vs. Fc^+/Fc)
1	-	+0.16
2	-2.25*	+0.40*/+0.97*,**
3	-2.41*	+0.19
4	-2.41*	+0.31
5	-2.42*	+0.35*

[a] E_{ox}°' refers to anodic process and E_{red}°' to cathodic process. Single asterisk (*) indicates that the process is irreversible (peak potential is given) and double asterisk (**) indicates the second peak of the wave.

On the cathodic side complexes **2**-**5** behave in a similar way, showing an irreversible process in the region between -2.25 and -2.42 V. In the case of **1**, the irreversible reduction is likely drown out by the solvent discharge.

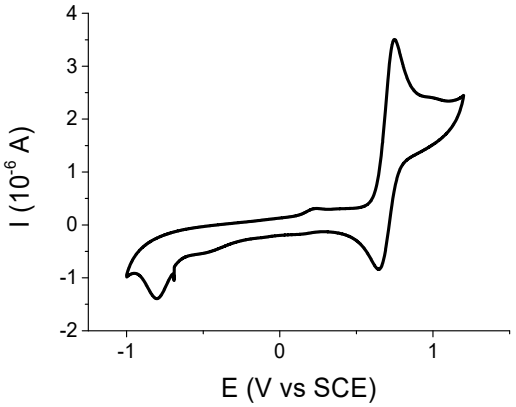

Figure 3. CV recorded in a 2mM solution (H_2O, phosphate buffer pH=2) of **2** at 50mV s^{-1}.

As described above, cyclic voltammetry of complex **1** suggests that the first process in the anodic side is mono-electronic. Indeed, the reactivity of complex **1** was studied by adding a stoichiometric amount of the one-electron oxidant "magic blue" (tris(4-bromophenyl)ammoniumyl hexachloroantimonate) at room temperature in THF, allowing the formation of a paramagnetic radical complex, isolated as a light yellow solid **1•** (Scheme 1).

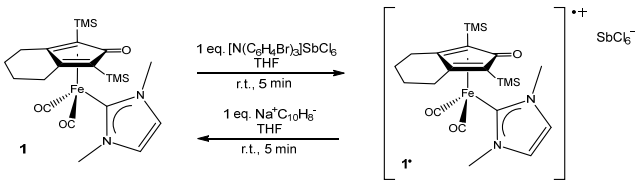

Scheme 1. Reversible generation of the radical complex **1•**.

The IR CO stretchings of radical species **1•** in THF solution shift to considerably higher values (**1** ν(CO) = 1983, 1922 cm^{-1} vs. **1•** ν(CO) = 2023, 1974 cm^{-1}), demonstrating an electron deficiency on the iron centre. Detection of the radical species by ESI-MS was performed by a spin trapping experiment: reaction with *N*-*tert*-butyl-α-phenylnitrone (PBN) yielded a more stable adduct, identified by ESI-MS at 686 m/z (Figure S22). Reaction of **1•** with an equivalent of sodium napthalenide regenerated the diamagnetic neutral species **1**.

The redox behavior of **1•** was studied by cyclic voltammetry and compared to **1** (Figure S2). Unfortunately in the case of **1•**, the investigation range is limited because of some redox processes that occur in the cathodic region and can be ascribed to the stripping of some adsorbed species. In fact, CV of **1•** exhibits a reversible redox process at + 0.073 V with a separation between the anodic and cathodic peaks that is higher than **1**, suggesting a slow charge transfer. Despite the little difference in the formal potential, Figure S2 suggests that the redox waves of **1** and **1•** involve the same species, hence highlighting that **1•** is the product of electrochemical oxidation of **1**.

EPR characterization

The paramagnetic nature of species **1•** was confirmed by recording EPR spectra of both solid and in solution samples (Figure S23). Room temperature THF solution of complex **1•** shows a sharp symmetric single peak (peak to peak line width 44.66 G), as expected for average anisotropies of the *g* tensor. An isotropic g value of 2.01247 was measured. Owing to the high stability of the complex we also measured the EPR spectrum of the solid sample directly at room temperature. Different *g* main components (g_x, g_y, g_z) were not observed in solid-state and the spectrum exhibits a single broader signal, (peak to peak line width 197.2 G), at a *g* value slightly higher than that observed in solution (g=2.01889). For transition metal complexes containing only one unpaired electron (S=1/2 systems), species with exact isotropic *g* values ($g_x=g_y=g_z$) are not possible because of Jahn–Teller distortions.[74] Therefore, the isotropic *g* value observed in solid is likely the result of unresolved g anisotropy due to poor resolution. The observation of sharp and strong EPR spectra of metal complexes in solutions at room temperature is usually an indication that the unpaired electron is located in a ligand-based orbital with only a partial mixing with metal orbitals. Actually, pure metal-centered radicals reveal a relatively large *g* anisotropy and their typical EPR spectra usually show *g* values higher than 2.10 or smaller than < 1.95.[74] The reported *g*-value in the solid (2.01889) supports the mixing of the unpaired electron with the iron metal orbitals in **1•**. Hyperfine splittings were not resolved both in solution and solid state. Therefore, information on the distribution of spin density was not possible. Mixing of **1•** with 5,5-dimethyl-1-pyrroline *N*-oxide (DMPO) (typically ca. 0.6 mM) led to the disappearance of the EPR signal due to **1•** and the recorded new spectrum consisted of three main spin-adducts. The first one, which disappeared in few minutes, was characterized by a_N=14.25 G, and a_H=18.31 G. These parameters are typical for carbon centered radical adducts.[75] The others two, which were found to be more persistent, were instead characterized by much smaller hydrogen coupling spectroscopic parameters consistent with adducts of oxygen radical species (a_N=13.10 G, a_H=10.03 G, a_N=12.35 G, and a_H=7.34 G).

DFT calculation

DFT calculations were carried out on complexes **1** and **4** and on the radical complex **1•**. Furthermore, in order to highlight the effect of the inclusion of the NHC ligand in the iron coordination shell, on the tris-carbonyl iron cyclopentadienone complex **6**.[57] Geometry optimization at the B3LYP level yielded overall structural features, bond lengths, and angles in good agreement with those available for complexes **1** and **4** observed by crystallography (See Table S2). The oxidation potential trend of compounds **6**, **1** and **4** from DFT studies confirms that measured from cyclic voltammetry. The ease of oxidation of the compounds was found to vary in the order: **6** > **4** > **1** as it appears from the calculated values of the energy of the highest occupied molecular orbital (HOMO) for each complex reported in Figure 4. In addition, HOMO energy are linearly correlated with the oxidation potentials (R^2 = 0.999 and slope = -0.93). Frontier molecular orbital pictures for complexes **6**, **1** and **4** are reported in panel a) of Figure 4 together with the corresponding energy values. The energy of the HOMO of complex **1** is significantly less negative than **6** indicating that it is easier to oxidize. HOMO energy value of complex **4** confirms that it is slightly more difficult to oxidize due to the presence of the electron withdrawing furan ring on the cyclopentadienone ligand.

Figure 4. Frontier molecular orbital diagrams HOMO (H) and LUMO (L) for a) **6**, **1**, **4** and c) **1•** complexes generated from DFT calculations, together with the corresponding plots of the orbital surfaces. In panel b) the spin density distribution in complex **1•** is reported: light blue and purple regions correspond to positive and negative values, respectively.

Only a small electron density resides on the NHC ligand in HOMO and LUMO of both **1** and **4** complexes. The electron

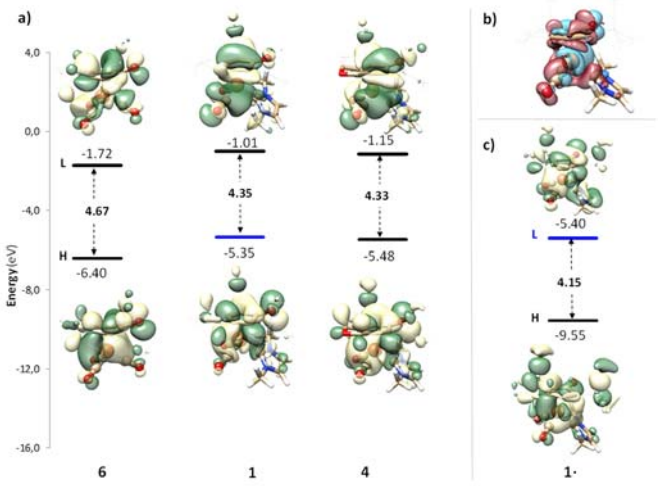

density is rather mainly located on the metal center and cyclopentadienone ligand of the complexes.

How the presence of the electron withdrawing furan ring on the cyclopentadienone ligand affects the properties of the complex has been checked by using both NBO analysis and CO ligand stretching frequencies. NBO second-order perturbation analysis reveals that metal-to-π* back-donation towards CO ligands is larger in **1** than in **4** (35.8 *vs* 33.2 and 33.7 *vs* 30.9 kcal mol^{-1} for the two CO ligands, respectively) due to the increased ability of cyclopentadienone ligand to draw electrons away from the metal, as confirmed also by the larger IR stretching frequencies for the CO ligands in **4** with respect to **1** (see Table S2) as well as

by the Fe-C=O bond distances that are slightly elongated in complex **4**.

Concerning the radical cationic complex **1•**, calculations show (see Figure 4 panel b) that the unpaired electron is shared between the iron centre and the cyclopentadienone ligand, with iron and ketone oxygen bearing the highest values (0.85 and 0.19, respectively) in substantial agreement with the EPR spectra. The comparison between the optimized structures of complexes **1** and **1•** confirms a significant elongation of three σ coordination bonds that Fe establishes with the ligands corresponding to a shortening of the bonds within each ligand. Accordingly, the CO IR stretching frequencies increase (see Table S2) as a consequence of the electron depletion on the iron centre.

Electro-catalytic activity of iron(0) Cyclopentadienone NHC complexes 1-5 for water oxidation

Once demonstrated that *N*-heterocyclic carbene ligands in cyclopentadienone iron complexes **1**-**5** exhibit an anodic monoelectronic process in a suitable potential region for water oxidation to O_2, their electrocatalytic properties were studied recording CVs in a THF/H_2O mixture (4:1, V/V), due to the low solubility of iron complexes **1**-**5** in water and the need of a solvent that can accept the protons generated by oxygen oxidation. First, the oxidation potentials registered in neutral THF/H_2O confirmed similar redox waves as in CH_3CN, at only slightly shifted potentials. The amino group plays a key role in the electrochemistry of the complexes also in this solvent mixture. The redox behavior of **2** and **5** is thoroughly discussed in the Supporting Information.

Then, choosing complex **1** as reference compound, CVs were recorded in the presence of increasing amounts of base (KOH). To our delight, an electrocatalytic behaviour was observed, as shown in Figure 5. In fact, the forward peak (positive I values) increases when the base is added to the solution, indicating that the neutral form of the complex is regenerated by the catalytic reaction pathway and can undergo a further oxidation step. At the same time, the backward peak decreases because the oxidized form of the complex is consumed and it cannot be reduced by the electrode.

The O_2 presence was firstly observed from the small bubbles clearly visible on the electrode surface when the oxidation was carried out with a large area electrode. The O_2 production was then demonstrated by enlarging the investigated potential range.

It is well-known that O_2 can be reduced at a GC electrode, and thus its signal should be visible in a cyclic voltammogram, after the occurrence of the electrocatalytic process.[76] Figure 5 shows the CV obtained in the aerated and de-aerated electrolytes and during the electrocatalytic process. The irreversible wave ascribable to O_2 reduction takes place at -1.13 V and it is clearly visible in the CV recorded in the aerated electrolyte solution. When O_2 is purged by N_2, its redox wave is no more present in the CV. The electrocatalytic water oxidation leads to O_2 production at the electrode surface, and thus two redox waves corresponding to the reduction to H_2O_2 and then to OH^- appear at potentials which are within the range of the broad system recorded for the aerated solution. The O_2 signal increases after each voltammetric cycle (Figure 6). Moreover, the higher the electrocatalytic current, the higher the current due to oxygen reduction, so confirming the correlation between the phenomena. The different shape of the redox waves, recorded in aerated electrolyte and during electrocatalysis, can be ascribed to the different pH of the electrolyte solution. In fact, the electrocatalysis is performed under basic conditions, while the electrolyte solution is neutral.

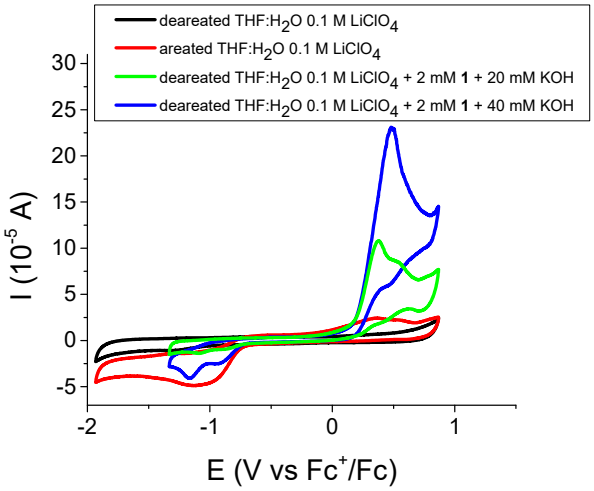

Figure 5. CVs (scan rate = 0.050 V s^{-1}) recorded at a glassy carbon electrode in THF/H_2O solutions highlighting O_2 generated by the electrocatalytic process. The scans started from the open circuit value and continued toward cathodic direction.

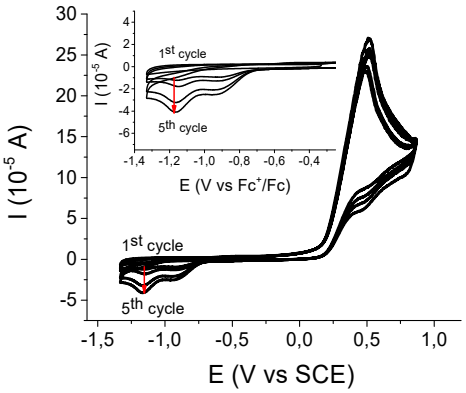

Figure 6. CVs (scan rate = 0.050 V s^{-1}) recorded at a glassy carbon electrode in THF:H_2O solutions containing 2 mM complex **1** and 40 mM KOH.

The ratio between the currents recorded in the presence (100 mM) and in the absence of potassium hydroxide, at a potential corresponding to the complex peak, was equal to 30. This value is so high as to rule out the possibility that the current is ascribable only to other possible reactions involving **1**, without the occurrence of a catalytic cycle. If *i*cat/*i*b (*i*cat=catalytic current, *i*b= blank current without substrate) is plotted vs KOH concentration, a linear increase of the catalytic current upon subsequent additions of base is observed, which is consistent

with a base-dependent mechanism for water oxidation (Figure 7).[77]

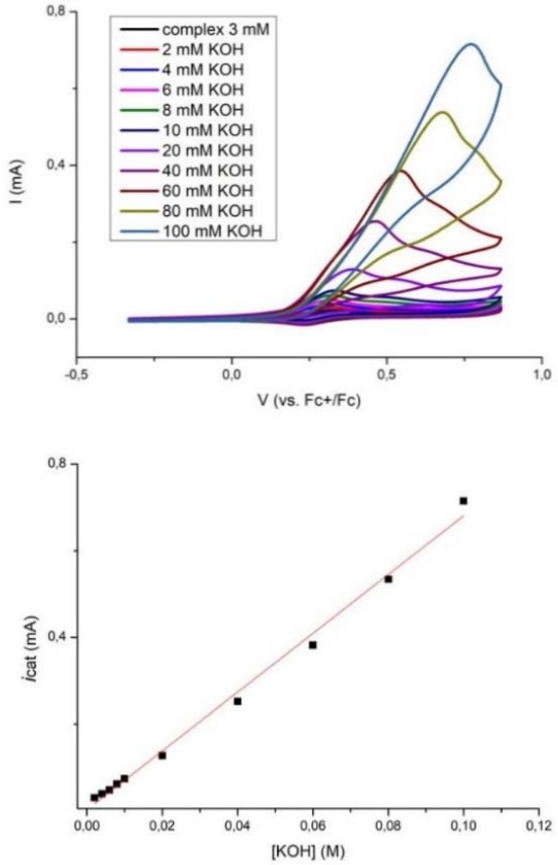

Figure 7. (Left) CVs in 3mM solution (THF/H_2O, 4:1) of **1** after subsequent KOH additions; scan rate: 50 mVs^{-1}. (Right) Increasing currents after base addition.

The CVs in Figure 7 are typical of a mixed behaviour, i.e. both kinetic and diffusion-controlled processes take place at GC electrode: the presence of the peak-shape confirms a diffusive regime, whilst the shifting to more anodic potentials of the peak current as the amount of substrate increase, is consistent with kinetic conditions. Since the control is not purely kinetic, the catalytic activity of **1** in terms of turn over frequency (TOF)[78] was calculated by a foot-of-the-wave analysis with the equation:

$$\frac{i_{cat}}{i_b} = \frac{2.242 n_{cat} (\frac{K_{cat} RT}{F\nu})^{\frac{1}{2}}}{1 + e^{(\frac{F}{RT}(E - E^0))}} \qquad (1)$$

where n_{cat} is the number of electrons involved in the catalytic reaction, K_{cat} is the pseudo-first-order rate constant, R is the universal gas constant, T is the temperature, F is the Faraday constant, E the potential, E^0 the standard potential of the redox mediator and v is the scan rate.

From the slope of the

$$\frac{i_{cat}}{i_b} vs \; {}^{1}\Big/_{1 + e^{(\frac{F}{RT}(E - E^0))}}$$

it is possible to calculate K_{cat}, which corresponds to the TOF value for O_2 evolution at the standard potential of the used catalyst. Calculation for **1** gives a TOF estimation of 52 s^{-1}.

Another parameter useful to evaluate the catalytic activity in voltammetry is the Catalytic Efficiency (C.E.) of the system,[79] which is given by

$$C.E. = \frac{i_{cat}/i_b}{C_B/C_{cat}}$$

In the equation, C_B is the base concentration and C_{cat} is the catalyst concentration. Thus, C.E. varies between 0 and 1, with 1 corresponding to the maximum efficiency. A plot of the ratio i_{cat}/i_b as a function of C_B/C_{cat} showed a linear correlation and C.E. was calculated for **1** to be 0.71.

On the basis of the results obtained for **1**, we discuss the behaviour of the other complexes bearing different substituted NHCs, i.e., **2** and **3**, and different cyclopentadienones, i.e., **4** and **5**. The electrocatalytic processes of **2** and **5** take place at the potential of the first wave observed in the first cycle, i.e., a potential that is lower than the peak potential reported for the redox couple. These data confirm that the complexes **2** and **5** are involved in acid/base equilibria that affect their redox behaviour. All complexes showed water oxidation activity upon addition of KOH to the solution (see Figure S3-6 for the corresponding CVs).

It is worth noting that for **1**, **3** and **4** the repeatedly recorded CVs demonstrated that the potential at which catalysis occurs is practically unchanged and the values are different for, and typical of, every single complex. These results strongly support that the first step of the reaction is the one electron oxidation of iron complexes, suggesting that no different species are responsible of electrocatalysis. The slopes of the plots of i_{cat}/i_b, TOF and C.E. values are reported in Table 2. The same Table reports also the formal potentials in THF/H_2O (4:1) of redox processes involving NHC-Cp=O iron complexes and the overpotential at which the oxygen evolution occurs with respect to the thermodynamic value of the couple O_2/OH^- (see Supporting Information for the calculation). All the values are comparable as suggested by a diffusive regime, but **1** and **3** display better performances as to TOF, C.E., and overpotential values. Furthermore, the reactivity as MWOCs is confirmed for the NHC-Cp=O iron systems.

Table 2. Slopes of i_{cat}/i_b , TOF and C.E. values for complexes **1-5**.

cat	$E_{ox}^{o'}$ (V vs. Fc^+/Fc)	Overpotential	Slope(i_{cat}/i_b)	TOF (s^{-1})	C.E.
1	+0.28	+0.32 V	$(3.6\pm0.1)10^2$	52	0.71
2	+0.42*/+0.64*,**		146±8	0.165	0.29
3	+0.29	+ 0.34 V	$(3.7\pm0.1)10^2$	28	0.73
4	+0.40	+ 0.45 V	200±5	10.6	0.42
5	+0.50*		231±1	11.7	0.46

* indicates that the process is irreversible (peak potential is given), and double asterisk ** indicates the second peak of the wave.

Finally, the role of KOH might be explained by two separated effects.

I. thermodynamic, by lowering the potential at which the O_2 evolution takes place at a particular pH. Indeed, in water the following equation E=E°-0.0592 pH holds, hence at basic pH conditions the oxygen will evolve at lower potential. In our THF/H_2O mixture, the OH^- concentration will exert the same effect on the reaction potential. Without base addition the reaction does not take place, as the by-product H^+ lowers pH in the absence of a buffer system and increases the reaction potential.

II. rate enhancement, as shown in Figure 7 for **1** (right), reporting the increase of the catalytic current (i_{cat}) versus KOH concentration.

Comparison with other electro-catalysts

Comparing complex **1** with other Fe or Ru based molecular systems for electrocatalytic water oxidation (Chart 2 and Table 3) it is clear that ruthenium catalysts still represent the best solution. Water soluble Ru-complexes that well perform under these conditions are, in fact, already available and, furthermore, they can be immobilized on the electrode surface: this is an important breakthrough toward real applications, since chemically modified electrodes are definitely better than homogeneous catalysts as far as recycle and reuse are concerned. On the other hand, very few examples of Fe complexes are reported in the literature as electrocatalytic WOCs and they mainly work as homogeneous catalysts in a mixture of water and organic solvent. Taking into consideration that Ru is not suitable for a large scale production, due to the high cost and low abundance, while Fe is a harmless and earth abundant element, there is still plenty of room for ligand design in order to improve Fe catalysts efficiency. Looking at Table 3, we can observe that the working potential of **1** is the lowest, but it must be emphasized that **1** cannot work in neutral or acidic solution, simply because the reaction is forbidden from a thermodynamic point of view. The overpotential of **1** is very close to the best value of the reported iron systems and it could be further improved by changing the pH of the electrolyte. From a kinetic point of view the TOF value of **1**, although competitive with the majority of the other available Fe electrocatalysts, is not very high. Anyway, it depends on the overpotential, as reported by Costentin et al.:[78] the higher the overpotential, the higher the TOF value, as demonstrated by the data reported in Table 3. It is worth noting that high overpotential values mean a high energy consumption in real applications, as a high voltage must be applied between the electrodes. In addition, our results clearly show that the overall reaction kinetics for **1** is limited by the diffusion at the electrode surface, since the redox wave exhibits a peak in CV. This means that the reaction kinetics is fast enough and other parameters could be optimized to boost oxygen evolution reaction.

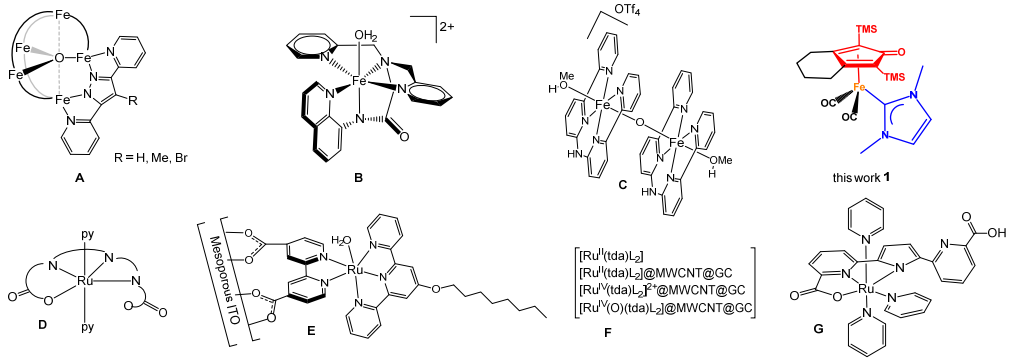

Chart 2. Literature available Fe and Ru based WOC catalysts.

Table 3 Summary of the performances of literature available electrocatalysts for WOC.

Complex	Ref.	Electrolyte + Reactant	TOF (s^{-1})	E	Overpotential (V)
A	51	ACN Et_4NClO_4 + Water	1900	1.08 V vs Fc^+/Fc	> 0.5
B	50	CAN 0.5 $LiClO_4$ + Water	0.015	1.58 V vs NHE	0.2 – 0.25
A	36	ACN TBAP (0.1 M) + Water	300	1.09 V vs Fc^+/Fc	0.65
C	53	Water Na_2SO_4	0.12	1.75 V vs RHE	0.3 – 0.4
D	80	pH 7 phosphate buffer	8000	1.43 V vs NHE	0.6
E	81	0.1 M KNO_3 solution pH 5.9	0.031	1.50 V vs Ag/AgCl	0.41
F	82	PBS pH 7	8935	1.45 vs NHE	0.634
G	83	pH 7	9400	1.25 vs NHE	0.434
Our cat **1**		THF:H_2O $LiClO_4$	52	0.28 vs Fc^+/Fc	0.32

Conclusions

In conclusion the ligands combination of cyclopentadienone and *N*-heterocyclic carbene on iron(0) carbonyl complexes demonstrated to promote, on one hand, the shift of the anodic process in a suitable potential region for oxidation of water to O_2, and, on the other hand, the mono-electronic oxidation/reduction of the complexes. This mono-electronic process leads, in oxidation, to the formation of an isolable and stable radical complex **1**$^{\bullet}$. The reaction is reversible, as also confirmed by electrochemical characterization of the mono-electronic redox processes of **1**, **3**, and **4**, unless when in the presence of a reactive NH_2 group in the lateral chain of the NHC ligand (**2** and **5** complexes). To our delight, despite the low formal metal valency, complexes **1**, **3**, and **4** were found to be stable, effective electrocatalysts for water oxidation in basic H_2O/THF mixtures. Both cyclopentadienone and NHC ligands were employed for the first time in the design of iron MWOC molecular catalysts and the simplest complex **1** showed the best catalytic activity and competitive efficiency in term of both TOF (up to 52 s^{-1}) and overpotential (320 mV). The versatility of both cyclopentadienone and NHC ligands in terms of steric and electronic control and their suitability toward the insertion of reactive functional groups could be exploited in order to improve water solubility and to chemically decorate the electrode with the electrocatalysts. This makes room for the design of more effective and/or immobilized iron based MWOCs toward the development of new green energy devices.

Author contributions

Methodology, Investigation and Validation: Andrea Cingolani and Cristiana Cesari (organometallic synthesis); Isacco Gualandi, Erika Scavetta (electrocatalysis); Stefano Zacchini (X-Ray Diffraction); Paola Franchi and Marco Lucarini (EPR analyses), Gloria Mazzone and Emilia Sicilia (DFT Calculation). Validation: Daniele Nanni (radical chemistry). Project administration, Conceptualization, Supervision: Rita Mazzoni. Writing original draft: Rita Mazzoni and Isacco Gualandi. Resourches and Funding acquisition: Valerio Zanotti and Domenica Tonelli.

Conflicts of interest

There are no conflicts to declare.

Acknowledgements

Authors wish to acknowledge University of Bologna for funding support.

Notes and references

1 A. Bard and M. A. Fox, *Acc. Chem. Res.*, 1995, **28**, 141-145.
2 T. J. Meyer, *Acc. Chem. Res.,* 1989, **22**, 163-170.
3 M. Yagi and M. Kaneko, *Chem. Rev.,* 2001, **101**, 21–36.
4 J. D. Blakemore, R. H. Crabtree and G W. Brudvig, G. W. *Chem. Rev.,* 2015, **115**, 12974–13005.
5 P. Garrido-Barros, C. Gimbert-Surinach, R. Matheu, X. Sala and A. Llobet, *Chem. Soc. Rev.,* 2017, **46**, 6088-6098.
6 M. D, Karkas, O. Verho, E. V. Johnston, and B. R. Akermark, *Chem. Rev.,* 2014, **114**, 11863–12001.
7 L: Duan, F. Bozoglian, S. Mandal, B. Stewart, T. Privalov, A. Llobet and L. Sun, *Nat. Chem.,* 2012, **4**, 418–423.
8 J. J. Concepcion, M. –K. Tsai, J. T. Muckerman and T. J. Meyer, *J. Am. Chem. Soc.,* 2010, **132**, 1545–1557.
9 V. Kunz, M. Schulze, D. Schmidt, and F. Wurthner, *ACS Energy Lett.,* 2017, **2**, 288–293.
10 D. W. Shaffer, Y. Xie, D. J. Szalda and J. J. Concepcion, *J. Am. Chem. Soc.,* 2017, **139**, 15347–15355.
11 L. Duan, L. Wang, F. Li and L. Sun, *Acc. Chem. Rev.,* 2015, **48**, 2084–2096.
12 J. D. Blakemore, N. D. Schley, D. Balcells, J. F. Hull, G. W. Olack, C. D. Incarvito, O. Eisenstein, G. W. Brudvig, and R. H. Crabtree, *J. Am. Chem. Soc.,* 2010, **132**, 16017–16029.
13 C. Wang, J. L. Wang, and W. Lin, *J. Am. Chem. Soc.,* 2012, **134**, 19895–19908.
14 A. Savini, G. Bellachioma, G. Ciancaleoni, C. Zuccaccia, D. Zuccaccia and A. Macchioni, *Chem. Commun.,* 2010, **46**, 9218–9219
15 G. Menendez Rodriguez, A. Bucci, R. Hutchinson, G. Bellachioma, C. Zuccaccia, S. Giovagnoli, H. Idriss and A. Macchioni, *ACS Energy Lett.,* 2017, **2**, 105−110.
16 D. J. Wasylenko, R. D. Palmer, E. Schott and C. P. Berlinguette, *Chem. Commun.,* 2012, **48**, 2107–2109.
17 K. Dogutan, R. McGuire and D. G. Nocera *J. Am. Chem. Soc.,* 2011, **133**, 9178–9180.
18 M. W. Kanan and D. G. Nocera, *Science,* 2008, 321, 1072–1075.
19 B. Zhang, F. Li, F. Yu, X. Wang, X. Zhou, X. Li, Y. Jiang and L. Sun, *ACS Catal.,* 2014, **4**, 804–809.
20 S. M. Barnett, K. I. Goldberg and J. M. Mayer, *Nat. Chem.,* 2012, **4**, 498–502.
21 M. T. Zhang, Z. Chen, P. Kang and T. J. Meyer, *J. Am. Chem. Soc.,* 2013, **135**, 2048–2051.
22 T. Ghosh, P. Ghosh and G. Maayan, *ACS Catal.,* 2018, **8**, 10631–10640.
23 P. Garrido-Barros, I. Funes-Ardoiz, S. Drouet, J. Benet-Buchholz, F. Maseras and A. Llobet, *J. Am. Chem. Soc.,* 2015, **137**, 6758–6761.
24 K. J. Fisher, K. L. Materna, B. Q. Mercado, R. H. Crabtree and G. W. Brudvig, *ACS Catal.,* 2017, **7**, 3384–3387.
25 Z. Chen and T. J. Meyer, *Angew. Chem., Int. Ed.,* 2013, **52**, 700–703.

26 R. E. Hansen and S. Das, *Energy Environ. Sci.,* 2014, **7**, 317–322.
27 E. A. Karlsson, B. -L. Lee, T. Akermark, E. V. Johnston, M. D. Karkas, J. Sun, O. Hansson, J.-E. Backvall and B. Akermark, *Angew. Chem., Int. Ed.,* 2011, **50**, 11715–11718.
28 L. Ma, Q. Wang, W. L. Man, H. K. Kwong, C. C. Ko and T. C. Lau, *Angew. Chem., Int. Ed.,* 2015, **54**, 5246–5249.
29 R. Brimblecombe, G. F. Swiegers, G. C. Dismukes and L. Spiccia, *Angew. Chem., Int. Ed.,* 2008, **47**, 7335–7338.
30 T. Ghosh and G. Maayan, *Angew. Chem., Int. Ed.,* 2019, **58**, 2785–2790.
31 T. Liu, B. Zhang and L. Sun, *Chem. Asian J.,* 2019, **14**, 31–43.
32 I. Roger and M. D. Symes, *J. Mater. Chem. A,* 2016, **4**, 6724–6741.
33 M. D. Karkas and B. Akermark, *Dalton Trans.,* 2016, **45**, 14421–14461.
34 A. R. Parent and K. Sakai, *ChemSusChem,* 2014, **7**, 2070–2080.
35 M. Kondo and S .Masaoka, *Chem. Lett.,* 2016, **45**, 1220–1231.
36 V. K. K. Praneeth, M. Kondo, M. Okamura, T. Akai, H. Izu and S. Masaoka, *Chem. Sci.,* 2019, **10**, 4628-4639.
37 W. C. Ellis, N. D. McDaniel, S. Bernhard and T. J. Collins, *J. Am. Chem. Soc.,* 2010, **132**, 10990–10991.
38 C. Panda, J. Debgupta, D. Diaz Diaz, K. K. Singh, S. S. Gupta and B. B. Dhar, *J. Am. Chem. Soc.,* 2014, **136**, 12273–12282.
39 S. Pattanayak, D. R. Chowdhury, B. Garai, K. K. Singh, A. Paul, B. B. Dhar, and S. S. Gupta, *Chem. Eur. J.,* 2017, **23**, 3414–3424.
40 E. P. Talsi and K. P. Bryliakov, *Coord. Chem. Rev.,* 2012, **256**, 1418–1434.
41 J. L. Fillol, Z. Codolà, I. Garcia-Bosch, L. Gjmez, J. J. Pla and M. Costas, *Nat. Chem.,* 2011, **3**, 807–813.
42 L. D. Wickramasinghe, R. Zhou,; R. Zong, P. Vo, K. J. Gagnon and R. P. Thummel, *J. Am. Chem. Soc*., 2015, **137**, 13260–13263.
43 W. A. Hoffert, M. T. Mock, A. M. Appel and J. Y. Yang, *Eur. J. Inorg. Chem.,* 2013, 3846–3857.
44 Z. Codolà, I. Garcia-Bosch, F. Acuca-Pars, I. Prat, J. M. Luis, M. Costas and J. Lloret-Fillol, *Chem. Eur. J.,* 2013, **19**, 8042–8047.
45 Z. Codolà, L. Gjmez, S. T. Kleespies, L. Jr. Que, M. Costas and J. Lloret-Fillol, *Nat. Commun.,* 2015, **6**, 5865.
46 P. Tan, H.-K. Kwong and T.-C. Lau, *Chem. Commun.,* 2015, **51**, 12189–12192
47 A. Annunziata, R. Esposito, G. Gatto, M. E. Cucciolito, A. Tuzi, A. Macchioni and F. Ruffo, *Eur. J. Inorg. Chem.,* 2018, 3304–3311.
48 W. P. To, T. W. S. Chow, C. W. Tse, X. Guan, J.S. Huang and C.M. Che, *Chem. Sci.,* 2015, **6**, 5891–5903.
49 A. R. Parent, R. H. Crabtree and G. W. Brudvig, *Chem. Soc. Rev.,* 2013, **42**, 2247–2252.
50 M. K. Coggins, M. T. Zhang, A. K. Vannucci, C. J. Dares and T. J. Meyer, *J. Am. Chem. Soc.,* 2014, **136**, 5531–5534.
51 M. Okamura, M. Kondo, R. Kuga, Y. Kurashige, T. Yanai, S. Hayami, V. K. Praneeth, M. Yoshida, K. Yoneda, S. Kawata and S. Masaoka, *Nature,* 2016, **530**, 465-468.
52 P. Pelosin, M. Gil-Sepulcre, P. Garrido-Barros, D. Moonshiram, J. Benet-Buchholz, C. Gimbert-Surinach, A. Llobet, *iScience*, **23**, 101378.
53 K. G. Kottrup, S. D'Agostini, P. H. van Langevelde, M. A. Siegler and D. G. Hetterscheid, *ACS Catal.,* 2018, **8**, 1052–1061.
54 S. Karim, A. Chakraborty, D. Samanta, E. Zangrando, T. Ghosh and D. Das *Catal. Sci. Technol.,* 2020, **10**, 2830-2837.
55 Z. Q. Wang, Z. C. Wang, S. Zhan and J. S. Ye, *Appl. Catal., A* 2015, **490**, 128–132.
56 M. M. Najafpour, R. Safdari, F. Ebrahimi, P. Rafighi and R. Bagheri, *Dalton Trans.,* 2016, **45**, 2618–2623.
57 A. Cingolani, C. Cesari, S. Zacchini, V. Zanotti, M.C. Cassani and R. Mazzoni, *Dalton Trans.,* 2015, **44**, 19063-19067.
58 Q. Liang and D. Song, *Chem. Soc. Rev.,* 2020, **49**, 1209-1232.
59 A. Quintard and J. Rodriguez, *Angew. Chem., Int. Ed.,* 2014, **53**, 4044 – 4055.
60 L. Pignataro and C.Gennari, *Eur. J. Org. Chem*., 2020, 3192–3205.
61 A. M. Oertel, V. Ritleng, L. Burr, C. Harwig and M. J. Chetcuti, *Organometallics,* 2011, **30**, 6685-6691.
62 L. M. Bushnell, E. R. Evitt and R. G. Bergman, *J. Organomet. Chem.,* 1978, **157**, 445-456.
63 A. Cingolani, V. Zanotti, S. Zacchini, M. Massi, P. V. Simpson, N. Maheshkumar Desai, I. Casari, M. Falasca, L. Rigamonti and R. Mazzoni, *Appl. Organomet. Chem.,* 2019, **33**, e4779.
64 S. Moulin, H. Dentel, A. Pagnoux-Ozheelyeva, S. Gaillard, A. Poater, L. Cavallo, J. F. Lohier and J. L. Renaud, *Chem. Eur. J.,* 2013, **19**, 17881-17890.
65 G. M. Sheldrick, SADABS, Program for empirical absorption correction, University of Göttingen, Germany, 1996.
66 G. M. Sheldrick, SHELX97, Program for crystal structure determination, University of Göttingen, Germany, 1997.
67 M. J. Frisch, G. W. Trucks, H. B. Schlegel, G. E. Scuseria, M. A. Robb, J. R. Cheeseman, G. Scalmani, V. Barone, B. Mennucci, G. A. Petersson, et al. Gaussian 09, Revision D.01; Gaussian, Inc.: Wallingford, CT, 2009.
68 D. Andrae, U. Haüssermann, M. Dolg, H. Stoll and H. Preuss, *Theor. Chim. Acta,* 1990, **77**, 123-141.
69 (a) J. E. Carpenter and F. J. Weinhold, *J. Mol. Struct.*, 1988, **169**, 41-62. (b) J. E. Carpenter and F. J. Weinhold, The Structure of Small Molecules and Ions; Plenum: New York, 1988
70 C. Cesari, S. Conti, S. Zacchini, V. Zanotti, M. C. Cassani and R. Mazzoni, *Dalton Trans.,* 2014, **4**, 17240-17243.
71 H. Allen, O. Kennard, D. G. Watson, L. Brammer, A. G. Orpen and R. Taylor, Tables of bond lengths determined by X-ray and neutron diffraction. Part 1. Bond lengths in organic compounds *J. Chem. Soc., Perkin Trans.,* 1987, **2**, S1-S19.
72 V. V. K. M. Kandepi, J. M. S. Cardoso, E. Peris and B. Royo, *Organometallics,* 2010, **29**, 2777-2782.
73 M. N. Hopkinson, C. Richter, M. Schedler and F. Glorius, *Nature,* 2014, **510**, 485–496.
74 Progress in Inorganic Chemistry, Vol. 55 Edited by Kenneth D. Karlin, John Wiley & Sons, Inc., 2007, 247-354.
75 J. L. Clément, B. C. Gilbert, A. Rockenbauer and P. Tordo, *J. Chem. Soc., Perkin Trans. 2*, 2001, 1463-1470.
76 J. R. Strobl, N. S. Georgescu and D. Scherson, *Electrochim. Acta,* 2020, **335**, 135432.
77 Z. Chen, J. J. Concepcion, X. Hu, W. Yang, P. H. Hoertz and T. J. Meyer, *PNAS* 2010, **107**, 7225-7229.
78 C. Costentin, S. Drouet, M. Robert and J. M. Saveant, *J. Am. Chem. Soc.* 2012, **134**, 11235−11242.
79 G. A. N. Felton, C. A. Mebi, B. J. Petro, A. K. Vannucci, D. H. Evans, R. S. Glass and D. L. Lichtenberger, *J. Organomet. Chem.* 2009, 694, 2681.
80 R. Matheu, M. Z. Ertem, J. Benet-Buchholz, E. Coronado, V. S. Batista, X. Sala and A. Llobet *J. Am. Chem. Soc.* 2015, **137**, 10786−10795.
81 Y. Tsubonouchi, J. Honta, T. Sato, E. A. Mohamed, Z. N. Zahran, K. Saito, T. Yui and M. Yagi, *Dalton Trans.* 2020, **49**, 1416–1423.
82 J. Creus, R. Matheu, I. Pecafiel, D. Moonshiram, P. Blondeau, J. Benet-Buchholz, J. Garcia-Anton, X. Sala, C. Godard and A. Llobet *Angew. Chem., Int. Ed.,* 2016, **55**, 15382 –15386.
83 R. Matheu, M. Z. Ertem, M. Pipelier, J. Lebreton, D. Dubreuil, J. Benet-Buchholz, X. Sala, A. Tessier and A. Llobet, *ACS Catal.,* 2018, **8**, 2039−2048.